

Nanoscale-SiC doping for enhancing J_c and H_{c2} in the Superconducting MgB_2

S. X. Dou*, V. Braccini**, S. Soltanian*, R. Klie***, Y. Zhu***, S. Li****, X. L. Wang*, and D. Larbalestier**

*Institute for Superconducting and Electronic Materials, University of Wollongong, Northfields Ave.
Wollongong, NSW 2522, Australia,

**Applied Superconductivity Centre, University of Wisconsin-Madison, USA and

***Brookhaven National Laboratory, Upton, NY, 11973, USA

****Advanced materials Research Centre, Nanyang Technological University, 639798, Singapore

The effect of nanoscale-SiC doping of MgB_2 was investigated using transport and magnetic measurements. It was found that there is a clear correlation between the critical temperature T_c , the resistivity ρ , the residual resistivity ratio, $RRR = R(300K)/R(40K)$, the irreversibility field H^* and the alloying state in the samples. SiC-doping introduced many nano-scale precipitates, provoking an increase of $\rho(40K)$ from $1 \mu\Omega\text{-cm}$ ($RRR = 15$) for the clean limit sample to $300 \mu\Omega\text{-cm}$ ($RRR = 1.75$) for the SiC-doped sample, leading to significant enhancement of H_{c2} and H^* with only minor effect on T_c . EELS analysis revealed a number of nano-scale impurity phases: Mg_2Si , MgO , MgB_4 , BO_x , $Si_xB_yO_z$, BC and unreacted SiC in the doped sample. TEM study showed an extensive domain structure of 2-4nm domains induced by SiC doping. The J_c for the 10% nano-SiC doped sample increased substantially at all fields and temperatures compared to the undoped samples, due to the strong increase in H_{c2} and H^* produced by SiC doping.

74.25.Sv, 74.25.Ha, 74.25.Fy, 74.70.Ad

Introduction

The critical current density (J_c) in MgB_2 has been a central topic for extensive research efforts since superconductivity in this compound was discovered¹. A number of techniques have been developed and employed to improve the J_c performance in magnetic fields. By using a chemical doping with nano-particle SiC into MgB_2 we have achieved a J_c enhancement in high fields by more than one order of magnitude, with only slight reduction in T_c ². A high density of nano-inclusions and possible substitution of SiC for B in MgB_2 was suggested to add effective pinning centers and raising $J_c(H)$ over a wide range of temperatures.

Recently, using high field transport measurements, Gurevich et al have reported the achievement of record high upper critical fields (H_{c2}) for high resistivity films and untextured bulk polycrystals³. They found that enhancements to the resistivity have a strong influence on H_{c2} . The observed remarkable H_{c2} enhancement to almost 50T is a consequence of the two-gap superconductivity of MgB_2 ³, which offers special opportunities for further H_{c2} increase by tuning the impurity scattering. Nanoscale SiC doping indeed introduces large alloying and potentially greatly raises resistivity too. Thus, we expected that transport measurements on SiC-doped samples would provide additional useful information for understanding the pinning mechanisms and upper critical field behavior of alloyed MgB_2 . In this paper we report on such transport and magnetic measurement evaluations in combination with TEM observations on the nanoscale-SiC doped MgB_2 .

Experimental Details

MgB_2 pellet samples were prepared by an in-situ reaction method, described in detail previously². Powders of magnesium (99%) and amorphous boron (99%) were well mixed with SiC nanoparticle powder (size of 10nm to 100nm) with the atomic ratio of MgB_2 with 10 wt% of SiC addition (sample B) and without (sample A). Pellets 10 mm in diameter and 2 mm in thickness were made under a uniaxial pressure sealed in the Fe tube and then heated at 800°C for 30min in flowing high purity Ar, followed by furnace cooling to room temperature. These two Wollongong samples were compared to two Madison samples, one being a clean limit (sample C) and the second being this same sample exposed to Mg vapor (sample D) as described in detail elsewhere⁴.

The resistivity versus temperature curves $\rho(T)$, were measured in magnetic fields up to 9 Tesla by a four-probe method at a current density of about 1 A/cm² using a 9 T Physical Property Measurement System (PPMS, Quantum Design). From the resistivity curves, we defined the upper critical field as $R(H_{c2})$

$= 0.9 R(T_c)$. We suppose that this critical field is that of the highest orientation, that is with H parallel to the Mg and B planes. Magnetization was measured from 5 to 30 K using an Oxford 14 T vibrating sample magnetometer (VSM). Bar-shaped Samples of about the same size were cut from the as-sintered pellets to minimize size-dependent effect⁵. Magnetic J_c values were determined from the magnetization hysteresis loops using the appropriate critical state model⁶. An empirical magnetic irreversibility line H_M^* was defined at the field at which J_c falls to 100 A/cm^2 ⁴. This corresponds we believe to the loss of full-sample connectivity close to H_{c2} perpendicular to the Mg and B planes (H_{c2}^\perp), since H^* is $\sim 0.9 H_{c2}$ ⁷. High-resolution transmission electron microscope (HRTEM) was employed to characterize the morphology of the samples. Electron energy loss spectroscopy (EELS)⁸ was obtained using a JEOL-3000F field emission STEM/TEM, equipped with a Schottky field-emission source operated at 300keV.

Results and Discussion:

Fig. 1 shows the resistivity curves $\rho(T)$ up to 9 T for the undoped (A) and the SiC-doped (B) samples. The onset T_c of the undoped sample was 37.5 K. For the 10wt% SiC-doped sample, T_c decreased only by 0.6K. By contrast, T_c is depressed to about 22K for C doped MgB_2 with nominal stoichiometry of $\text{Mg}(\text{B}_{0.8}\text{C}_{0.2})_2$ synthesized from Mg and B_4C ⁹. These results suggest little if any C substitution for B in the doped sample. It is also clear that the doped sample has stronger superconductivity than the undoped, as is shown explicitly in Fig. 2, where the 90% values of the resistive transitions from Fig. 1 are shown. A further important point is that the nominal resistivities of the two samples are very different, $\rho(40\text{K})$ being $90 \mu\Omega\text{cm}$ for the undoped sample and $300 \mu\Omega\text{cm}$ for the doped sample. We consider that the 90% transition approximates H_{c2}^\parallel . Fig.2 also includes the same data taken on the clean-limit ($\rho(40\text{K}) = 1 \mu\Omega\text{cm}$) and Mg-exposed sample ($\rho(40\text{K}) = 18 \mu\Omega\text{cm}$) of Braccini et al. [4]. The clean limit ($\rho(40\text{K}) = 1 \mu\Omega\text{cm}$) and the undoped samples have H_{c2}^\parallel values of 3.1 and 3.3 T at 30K, while the Mg-exposed ($\rho(40\text{K}) = 18 \mu\Omega\text{cm}$) and SiC-doped are respectively 5.1 and 4.6 T at 30 K. Since H_{c2} should be directly tied to ρ it is clear percolative normal state effects must be considered to be affecting the derived values of resistivity, which are not directly interpretable as being representative of the scattering in the samples.

Fig. 3 shows the $J_c(H)$ curves for the undoped and SiC-doped MgB_2 samples at 4.2K, 10K, 20K and 30K. Consistent with its higher H_{c2} , the doped sample shows smaller dependence of J_c on magnetic field at all temperatures. At 4.2K and low field both samples attain about 10^5 A/cm^2 , while falling to 100 A/cm^2 at 12T and 9T at 10K and 7.4T and 5.6T at 20K for doped and undoped samples, respectively. Both samples show a similar exponential fall-off of J_c with increasing field. Fig. 4 shows that the J_c values for the Wollongong samples are higher than for the two Madison samples, perhaps because the latter samples have

about 40% porosity [4]. At 20K, the 10wt% SiC doped sample achieved 10^5A/cm^2 at 3T, comparable to that of state-of-the-art Ag/Bi-2223 tapes and an order of magnitude higher than recent state-of-the-art Fe/MgB₂ tapes¹⁰. These results significantly strengthen the position of MgB₂ as a competitor for both low and high temperature superconductors.

The irreversibility fields (H_{M^*}), derived from the fields at which the magnetic hysteresis loops obtained with the VSM indicate that $J_c = 100 \text{A/cm}^2$ are shown in Fig. 5. We believe that H_{M^*} corresponds to about 90% of H_{c2}^\perp . Doping with SiC significantly improved H_{M^*} . For example, the H_{M^*} for the SiC doped sample reached 7.4T, compared to 5.6T for the undoped one, 5.2T for the Mg vapour treated one and 3.8T for the clean limit one at 20K.

To understand the significant enhancement of J_c at higher fields for the nano-SiC doping we compare the resistivity ρ and residual resistivity ratio (RRR) for sample A and B, as shown from the resistivity versus temperature curves reported in Fig. 6. For comparison we list some literature data in Table 1. The highest value of H_{M^*} correlates well to the highest value of resistivity, both being found in the SiC-doped sample for which the $J_c(H)$ characteristics are best too. This correlation is not found for all samples. However, as Rowell¹¹ has recently shown, many measurements of resistivity do not yield values that are characteristic of the local scattering processes which control H_{c2} ¹². The reasons for this is that most samples are less than fully connected, due to the presence of significant sample porosity, cracks or wetting, insulating phases at grain boundaries. In the general case the magnitude of these issue is unknown. In the present case it is interesting that samples A and D in Table 1 have rather similar T_c (37.2 and 36.9K) and H_{M^*} (5.5 and 5.0T at 20K). However, their resistivity values are wildly different ($\rho(40\text{K}) = 90$ and $18 \mu\Omega\text{cm}$), quiet unrepresentative of the actual scattering processes which really determine H_{c2} and H^* .

| Sample | A: Undoped | B: SiC doped | C: Clean limit | D: Mg vapor treated | Pure bulk (Ref. 13) |
|----------------------------------|------------|--------------|----------------|---------------------|---------------------|
| T_c (K) | 37.2 | 36.5 | 39 | 36.9 | 40.2 |
| ρ ($\mu\Omega$ -cm) at 40K | 90 | 300 | 1 | 18 | 1 |
| RRR R(300K)/R(40K) | 2.1 | 1.74 | 14.7 | 3 | 19.7 |
| H_m^* (20K) (T) | 5.6 | 7.4 | 3.9 | 5.2 | 3.8 |

Table 1. Comparison of T_c , resistivity and irreversibility field data for samples A, B, C, D and one literature sample (sintered pellet made from $^{10}\text{B}^{13}$).

Recently, Gurevich et al.³ has reported a record-high $H_{c2}(0) = 29\text{T}$ for untextured sample C and $H_{c2}^{\perp}(0) = 34\text{T}$ and $H_{c2}^{\parallel}(0) = 49\text{T}$ for a high resistivity film ($\rho(40\text{K}) = 220 \mu\Omega\text{cm}$) using direct, high-field resistivity measurements³. In this study, sample D in Table 1 above was measured after aging for two months, during which time the resistivity, ρ , dropped from its original value of 18 to 5 $\mu\Omega$ -cm at 40K, while T_c also increased from 36.9 K to 37.7 K, due probably to relaxation of a quenched defect

structure. A clean film with a low resistivity of 7 $\mu\Omega$ -cm at 40K had H_{c2}^{\parallel} of 29T, in comparison to the 49T of the 220 $\mu\Omega\text{cm}$ film. It seems likely that the SiC-doped sample with the highest resistivity of 300 $\mu\Omega$ -cm will also have a very high H_{c2} , at least equal to that of the Mg-vapour-treated sample D.

The TEM examination revealed that there is a number of impurity phases in the form of nano-meter size inclusions inside and in between grains in the nano-SiC doped sample. These impurities include Mg_2Si , MgB_4 and MgO detected by XRD analysis^{2,14}, and unreacted SiC, amorphous BO_x , $\text{Si}_x\text{B}_y\text{O}_z$ and BC detected by using EELS technique. TEM images show that the grain size of MgB_2 is smaller than 100nm. EDX analysis shows that the Mg:Si ratio is identical across the entire sample, indicating that the phase distribution is globally homogeneous. However, nano-scale impurity phases MgB_4 and MgO are present within the grains. The presence of oxygen within grains is consistent with the results obtained from the above-mentioned 220 $\mu\Omega\text{cm}$ thin film with strong pinning where the ratio of Mg:B:O reached 1.0:0.9:0.7¹⁵. Fig. 7 is a TEM image showing some unreacted SiC particles and its lattice image. The EELS analysis (convergence angle (α) = 13 mrad, collection angle (θ_c) = 18 mrad) shows that this particle is indeed pure SiC without B or any other element in it. The EELS analyses also show other phases present in the SiC doped sample. Fig. 8 (a) shows the EELS spectrum of the $\text{Si}_x\text{B}_y\text{O}_z$ phase with no C. Both the fine-structure of Si and B suggests that the phase is amorphous. Fig. 8(b) is the EELS spectrum of the BC

phase. Again, the fine-structure of B suggests that the phase is amorphous. The EELS of amorphous BO_x is shown in Fig. 8(c). These phases are often seen between two grains of MgB_2 in the sample.

Based on lattice parameter changes and EDX analysis we suggested that C and Si might substitute into the lattice in an early work². However, recent work on SiC-doped MgB_2 single crystal grown under high pressure (30 kbar) and high temperature (1900-1950°C) showed there was only C substitution for B but no Si detected in the crystals. These authors revealed that the C substitution for B is as high as 16%, the highest level of substitution in all the C-doping studies so far¹⁶. There is a clear trend for the C substitution in MgB_2 in the literature data^{17,18,19,20}. The higher the sintering temperature is the larger proportion of C is substituted for B in MgB_2 . As we used relatively lower sintering temperature the C substitution for B is expected to be lower. For the nano-SiC doped sample, Fig. 9 (a) is the Z-contrast image^{21,22,23}, which shows a typical MgB_2 crystal in the [100] orientation. A close up look of the atomic structure of the high-resolution lattice image shows that only the Mg columns are visible (Fig. 9(b)), due to the small scattering amplitude of B²⁴. The EELS shows the typical fine-structure for B in MgB_2 ²⁴, but no C signal can be detected (Fig. 9(c)). It should be noted here that light elements, such as C or B can be detected in concentrations down to 0.2% with 10% accuracy in a matrix such as MgB_2 . However, it is rather difficult to distinguish a small C signal originating from within the lattice or from surface contamination, as the low signal-to-noise ratio of the C core-loss for such low concentrations makes it nearly impossible to distinguish the near-edge fine-structure. Due to the large variety of phases present in the SiC doped sample, it is therefore possible that the C substitution at level 1-3%, which is believed to be quite reasonable from the frame work of literature on C substitution¹⁶⁻²⁰, can not be readily identified, and more careful analysis is needed.

In addition to the high concentration of the nano-inclusions, there are structural defects observed in the nano-SiC doped sample. Fig. 10 shows a high resolution TEM image of the morphology of the SiC doped sample. The majority of nano-domains have a rectangular shape with a domain size of about 2-4 nm. The domain boundaries trap numerous defects to form nano-defect wells and release the strain caused by the rotation of nanodomains, as reported by Li et al²⁵. This nano-domain structure may be the result of a small proportion of C substituted for B. In our recent work, we found that C substitution indeed improved flux pinning, while also depressing T_c . It was found that an optimal combination of substitution and addition achieved the best enhancement of flux pinning²⁶.

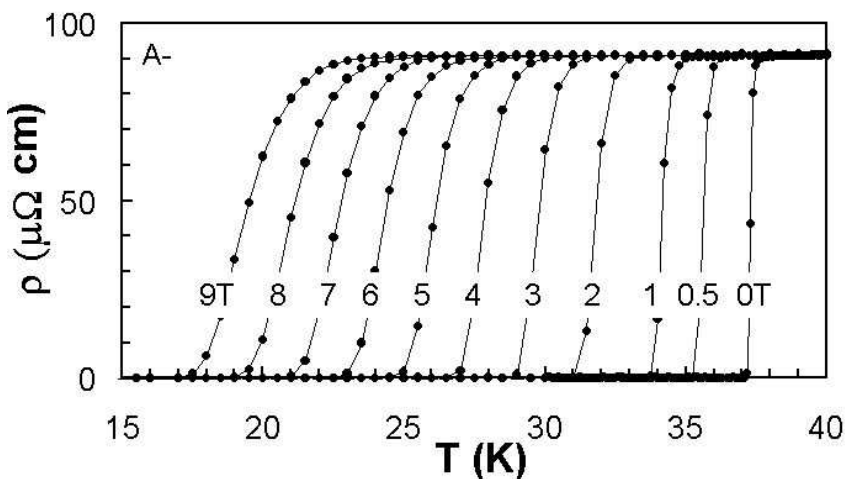
Conclusion

We have demonstrated that nano-scale SiC doping into MgB₂ introduces a high concentration of various nano-scale impurity phases which results in a very high resistivity, low residual resistivity ratio and large irreversibility field and upper critical field with modest T_c reduction. The highly dispersed nanoscale precipitates do not appear to cause weak links and may serve as strong pinning centres. The doping with SiC shows enhanced critical current density, irreversibility field and upper critical field in a manner helps make MgB₂ potentially competitive with both low and high-T_c superconductors.

Acknowledgment

The authors thank J. Horvat, M.J. Qin, A. Pan, M. Ionescu, H.K. Liu, S.H. Zhou, L.D. Cooley, M. Tomsic and E.W. Collings for their help in various aspects of this work. The work in Wollongong was supported by the Australian Research Council, Hyper Tech Research Inc OH USA, Alphatech International Ltd, NZ and the University of Wollongong, while that in Madison was supported by NSF through the MRSEC on Nanostructured materials and interfaces.

Fig. 1. The resistivity vs. temperature in fields up to 9 T for the undoped (A) and SiC-doped (B) samples.



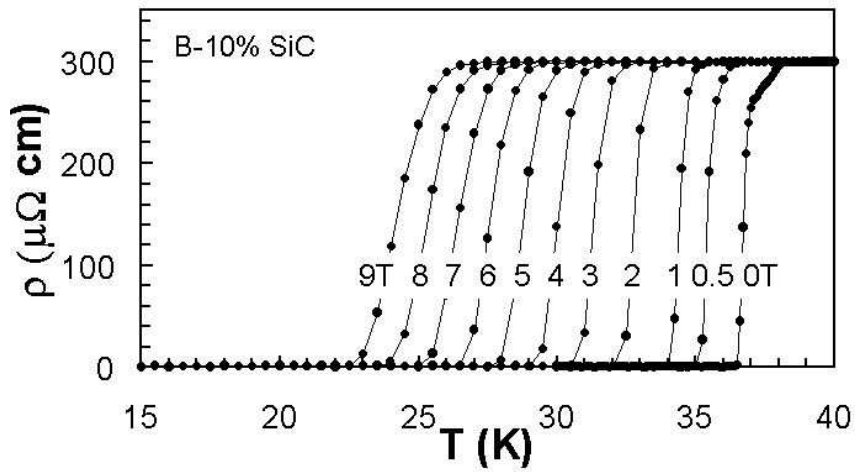


Fig. 2. The 90% of the resistive transition (upper critical field) as a function of the temperature for the undoped (A), the 10wt% SiC doped sample (B), the clean limit (C) and the Mg vapor treated (D) samples .

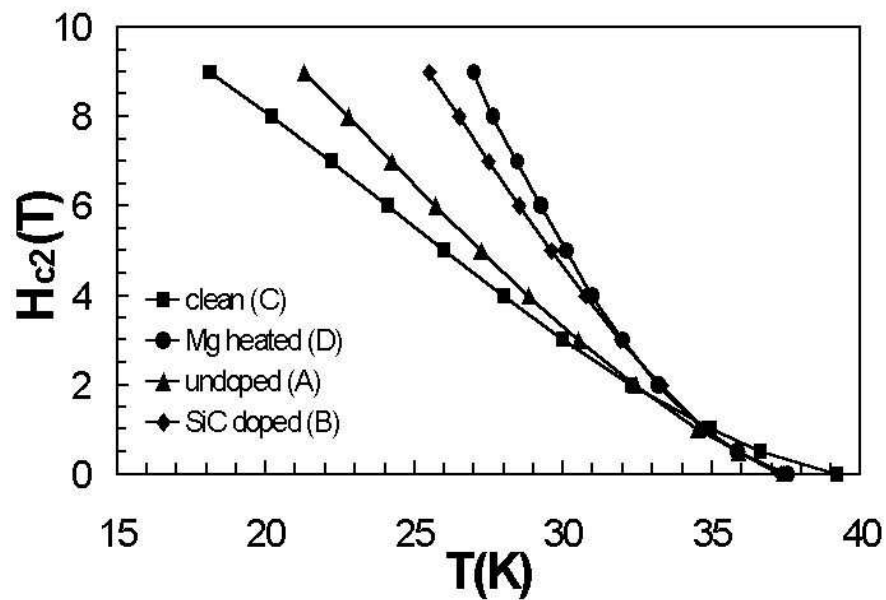


Fig. 3. The $J_c(H)$ at 4.2, 10, 20 and 30 K for the undoped (A) and SiC doped (B) samples.

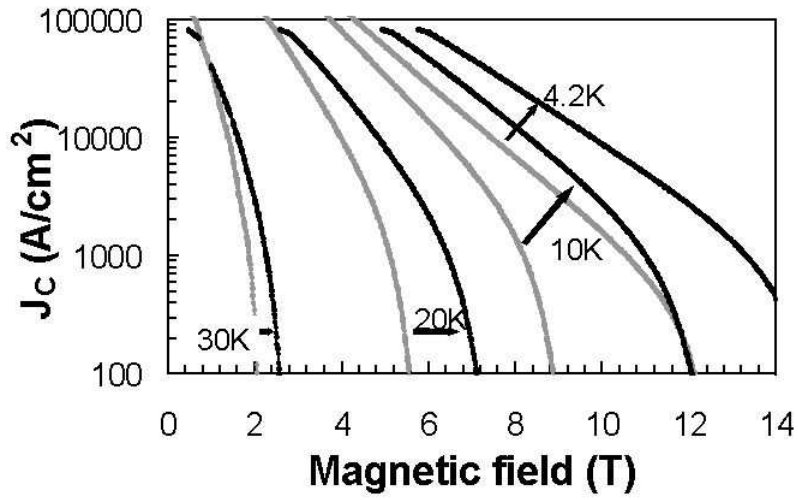
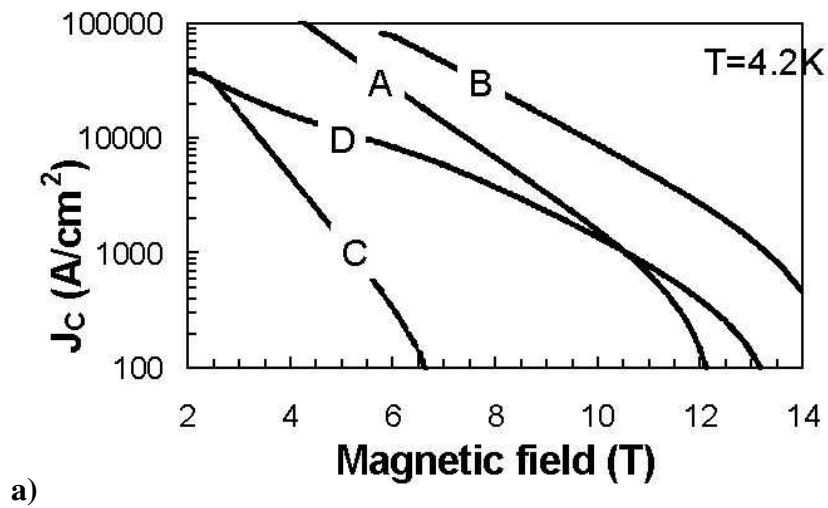
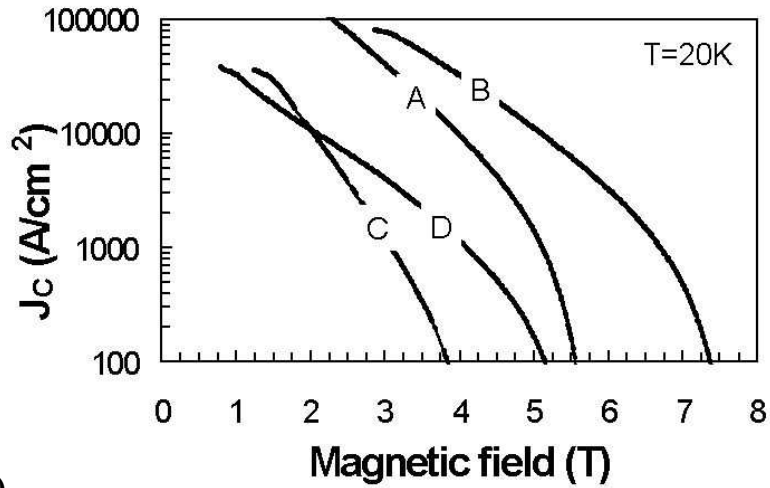


Fig. 4. A comparison of $J_c(H)$ for the undoped (A), 10wt% SiC doped sample (B), the clean limit (C) and the Mg vapor treated (D) samples at 4.2 K (a) and 20K (b)





b)

Figure 5: The irreversibility field, H_M^* vs. temperature for the samples A, B, C and D

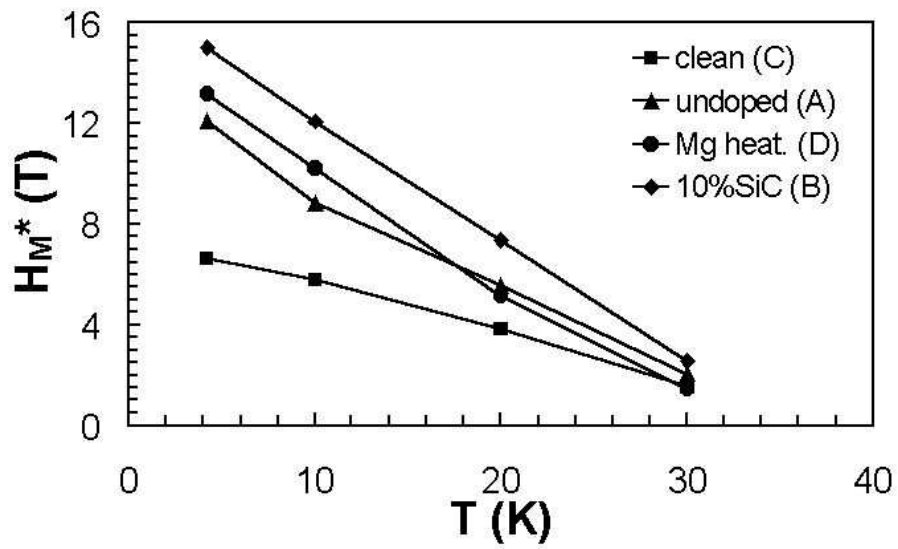
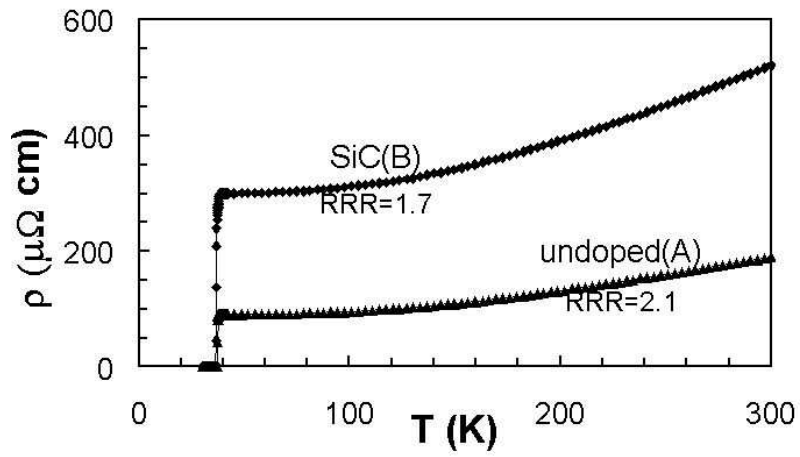


Figure 6: The resistivity curve as a function of the temperature at zero field for the undoped (A) and SiC-doped (B) samples in the full range 30-300K (a) and near T_c (b)

a)



b)

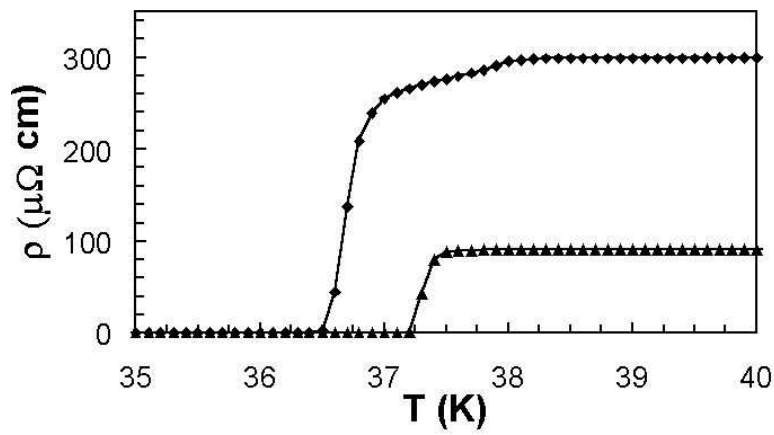
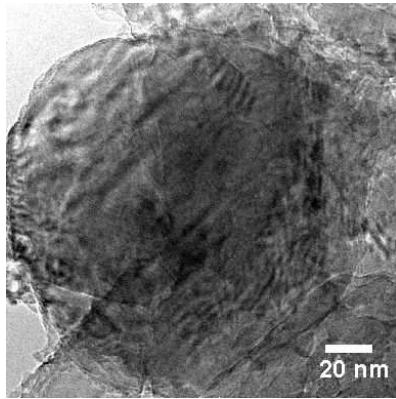
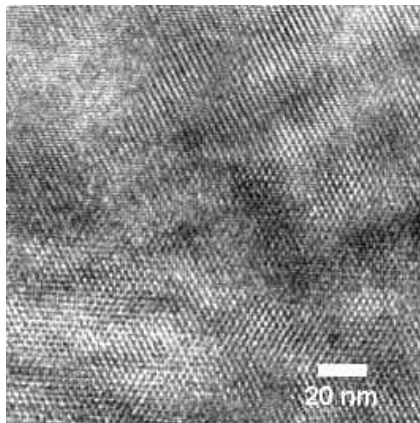


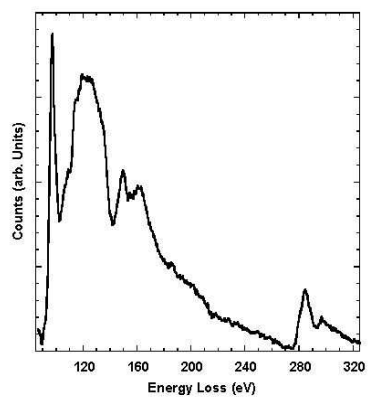
Figure 7: Conventional TEM image of an unreacted SiC particle; b) high-resolution TEM image of the bulk of the SiC particle and c) EELS spectrum clearly showing the Si L- and the C K-edge.



a)



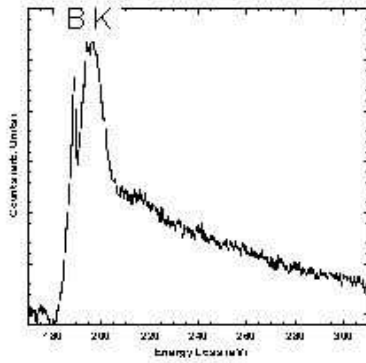
b)



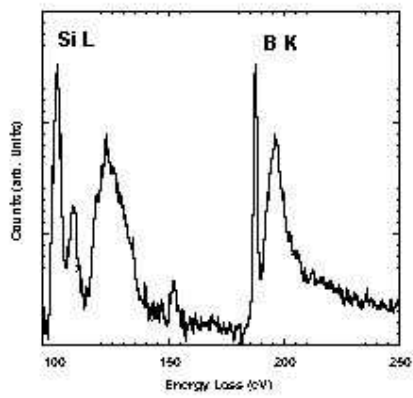
c)

Figure 8: The EEL spectrum of amorphous a) BO_x , b) $\text{Si}_x\text{B}_y\text{O}_z$ and c) BC detected in the SiC doped MgB_2 .

a)



b)



c)

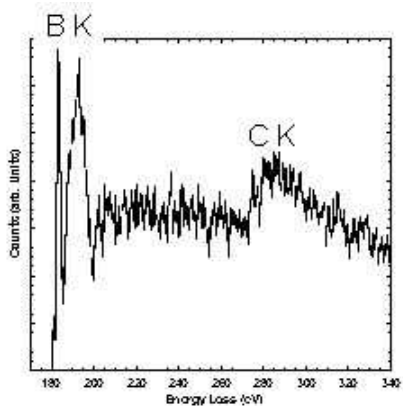
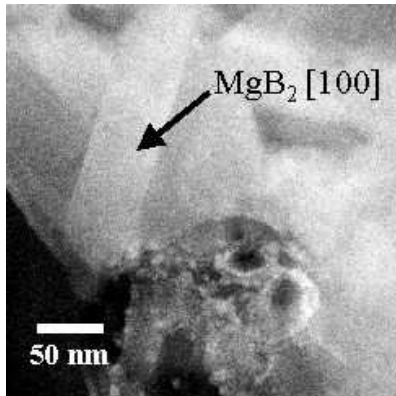
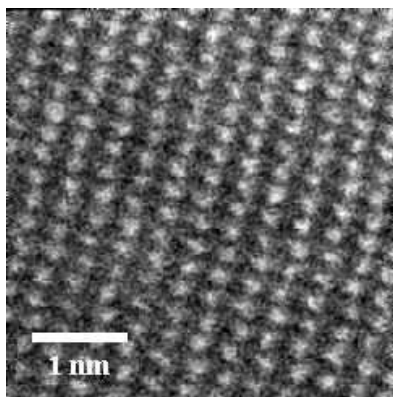


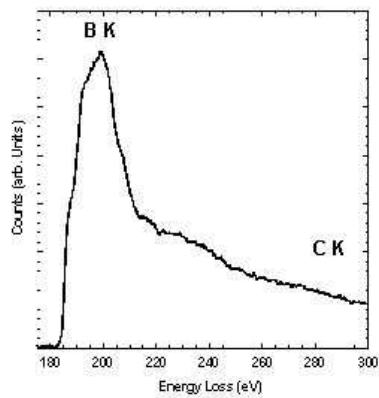
Figure 9 a) The Z-contrast image of a typical MgB_2 grain in the [100] orientation; b) high-resolution Z-contrast image of the bulk of the MgB_2 grain showing the Mg columns only and c) EELS spectrum of of the B K-edge from the MgB_2 grain.



a)

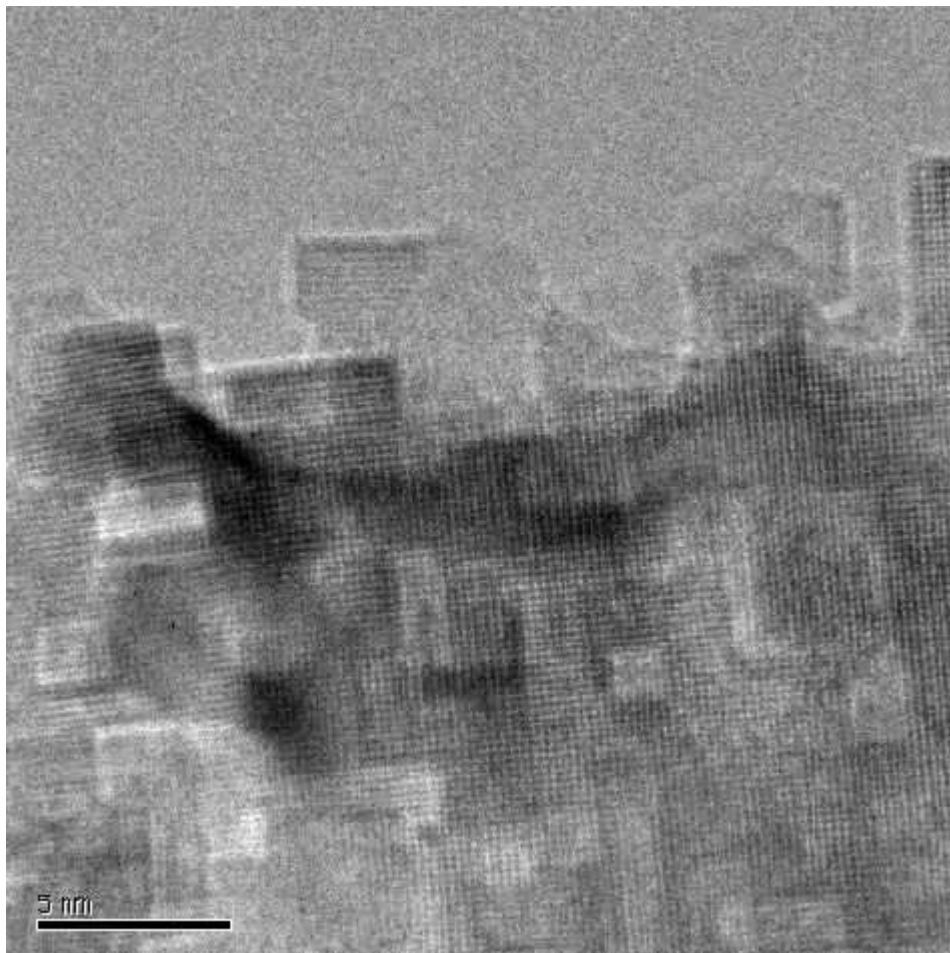


b)



c)

Figure 10: HRTEM image of nano-domain structure with rectangular nano-wells in the SiC-doped sample (B)



¹ J. Nagamatsu, N. Nakagawa, T. Muranaka, Y. Zenitani and J. Akimitsu, *Nature* **410**, 63 (2001).

² S. X. Dou, S. Soltanian, X. L. Wang, P. Munroe, S. H. Zhou, M. Ionescu, H. K. Liu, and M. Tomsic, *Applied Physics Letter* **81**, 3419 (2002).

³ A. Gurevich, S. Patnaik, V. Braccini, K. H. Kim, C. Mielke, X. Song, L. D. Cooley, S. D. Bu, D. M. Kim, J. H. Choi, L. J. Belenky, J. Giencke, M. K. Lee, W. Tian, X. Q. Pan, A. Siri, E. E. Hellstrom, C. B. Eom, D. C. Larbalestier, *Cond-mat* 0305474.

-
- ⁴ V. Braccini, L. D. Cooley, S. Patnaik, D. C. Larbalestier, P. Manfrinetti, A. A. Palenzona, and A. S. Siri, *Appl. Phys. Lett.* **81**, 4577 (2002).
- ⁵ J. Horvat, S. Soltanian, X. L. Wang, and S. X. Dou, cond-mat/0304004.
- ⁶ J. E. J. E. Evetts, *Concise Encyclopedia of Magnetic and Superconducting Materials* (Pergamon, New York, 1992), p.99.
- ⁷ S Patnaik, L. D Cooley, A Gurevich, A. A. Polyanskii, J. Jiang, X. Y. Cai, A. A. Squitieri, M. T. Naus, M. K. Lee, J. H. Choi, L. Belenky, S. D. Bu, J. Letteri, X Song, D. G. Schlom, S. E. Babcock, C. B. Eom, E. E. Hellstrom, and D. C. Larbalestier, *Sup. Sci. Tech.* **14**, 2001 (315).
- ⁸ R. F. Egerton, *Electron Energy Loss Spectroscopy in the electron microscope* (Plenum, New York, 1986)
- ⁹ R.A Ribeiro, S. Budko, C. Petrovic, and P. C. Canfield, *Physica C* **384**, 227 (2003).
- ¹⁰ R. Flukiger, H. L. Suo, N. Mugolino, C. Benedice, P. Toulemonde, and P. Lezza, *Physica C* **385**, 286 (2003).
- ¹¹ J. M. Rowell, *Supercond. Sci. Technol.* **16**, R17 (2003).
- ¹² A. Gurevich, *Phys. Rev. B* **67**, 184515 (2003).
- ¹³ D. K. Finnemore, J. E. Ostenson, S. L. Bud'ko, G. Lapertot, and P. C. Canfield, *Phys. Rev. Lett.* **86**, 2420 (2001).
- ¹⁴ S. X. Dou, A. V. Pan, S. Zhou, M. Ionescu, H. K. Liu, and P. R. Munroe,, *Supercond. Sci. Technol.* **15**, 1 (2002).
- ¹⁵ C. B. Eom, M. K. Lee, and J. H. Choi, L. J. Belenky, X. Song, L. D. Cooley, M. T. Naus, S. Patnaik, J. Jiang, M. Rikel, A. Polyanskii, A. Gurevich, X. Y. Cai, S. D. Bu, S. E. Babcock, E. E. Hellstrom, D. C. Larbalestier, N. Rogado, K. A. Regan, M. A.

-
- Hayward, T. He, J. S. Slusky, K. Inumaru, M. K. Haas, and R. J. cava, *Nature* **411**, 558 (2001).
- ¹⁶ S. M. Kazakov, J. Karpinski, J. Jun, P. Geiser, N. D. Zhigadlo, P. Puznak, and A. V. Mironov, *Cond-mat/0304656*.
- ¹⁷ T. Takenobu, T. Ito, Dam Hieu Chi, K Prassides, and Y. Iwasa,, *Phys. Rev. B* **64**, 134513 (2001).
- ¹⁸ I. Maurin, S. Margadonna, K. Prassides, T Takenobu, Y Iwasa, and A. N. Fitch, *Chem. Mater.* **14**, 3894 (2002).
- ¹⁹ W. Mickelson, J. Cumings, W. Q. Han, and A Zettl, *Phys. Rev. B* **65**, 052505 (2002).
- ²⁰ Z. H. Cheng and B.G. Shen et al., *J. Appl. Phys.* **91**, 7125 (2002).
- ²¹ E. M. James and N.D. Browning, *Ultramicroscopy* **78**, 125 (1999).
- ²² N. D. Browning, M. F Chrisholm, and S. J. Pennycook, *Nature* **366**, 143 (1993).
- ²³ G. Duscher, N. D. Browning, and S. J. Pennycook, *Physica Status Solidi* **166**, 327 (1998).
- ²⁴ R. F. Klie, J. C. Idrobo, N. D. Browning, K. A. Regan, N. S. Rogado, and R. J. Cava, *Appl. Phys. Lett.* **79**, 837 (2001).
- ²⁵ S. Li, T. White, K. Laursen, T. T. Tan, C. Q. Sun, Z. L. Dong, Y. Li, S. H. Zhou, J. Horvat, and S. X. Dou, *Appl. Phys. Lett.* **83**, 314 (2003).
- ²⁶ S. X. Dou, W. K. Yeoh, J. Horvat, and M Ionescu, submitted.